PASJ: Publ. Astron. Soc. Japan **59**, S771–S778, 2007 November 30

A Study of Polar Jet Parameters Based on Hinode XRT Observations

Antonia SAVCHEVA, Jonathan CIRTAIN, Edward E. DELUCA, Loraine L. LUNDQUIST, Leon GOLUB, and Mark WEBER
Harvard-Smithsonian Center for Astrophysics, 60 Garden St., Cambridge, MA 02139, USA
asavcheva@cfa.harvard.edu
Masumi SHIMOJO and Kiyoto SHIBASAKI
Nobeyama Solar Radio Observatory, NAOJ, Nobeyama, Nagano, 384-1305
Taro SAKAO and Noriyuki NARUKAGE
Institute of Space and Astronautical Science, Japan Aerospace Exploration Agency,
3-1-1 Yoshinodai, Sagamihara, Kanagawa 229-8510
and
Saku TSUNETA and Ryouhei KANO
National Astronomical Observatory of Japan, 2-21-1 Osawa, Mitaka, Tokyo 181-8588

(Received 2007 May 31; accepted 2007 September 11)

Abstract

Hinode/SOHO campaign 7197 is the most extensive study of polar jet formation and evolution from within both the north and south polar coronal holes so far. For the first time, this study showed that the appearance of X-ray jets in the solar coronal holes occurs at very high frequency — about 60 jets d^{-1} on average. Using observations collected by the X-Ray Telescope on Hinode, a number of physical parameters from a large sample of jets were statistically studied. We measured the apparent outward velocity, the height, the width and the lifetime of the jets. In our sample, all of these parameters show peaked distributions with maxima at $160\,\mathrm{km\,s^{-1}}$ for the outward velocity, 5×10^4 km for the height, 8×10^3 km for the width, and about 10 min for the lifetime of the jets. We also present the first statistical study of jet transverse motions, which obtained transverse velocities of 0–$35\,\mathrm{km\,s^{-1}}$. These values were obtained on the basis of a larger (in terms of frequency) and better sampled set of events than what was previously statistically studied (Shimojo et al. 1996, PASJ, 48, 123). The results were made possible by the unique characteristics of XRT. We describe the methods used to determine the characteristics and set some future goals. We also show that despite some possible selection effects, jets preferably occur inside the polar coronal holes.

Key words: Sun: activity — Sun: corona — Sun: magnetic field

1. Introduction

In the early nineties the Yohkoh mission clearly showed that reconnection events, and more specifically X-ray jets, play an important part in coronal dynamics (Shimojo et al. 1996; Shibata et al. 1992; Strong et al. 1992). Simple models of magnetic reconnection between different configurations (anemone, arcades, etc.) of confined closed fields and the open field of the corona have been employed to explain the emergence of jets. Different mechanisms explaining the subsequent ejection of material and the propagation of the jet are still frequently discussed. Chromospheric evaporation flows, conduction fronts, and magnetic acceleration of expanding plasma are usually considered (Shimojo et al. 1996; Shibata et al. 1992; Canfield et al. 1996; Alexander & Fletcher, 1999). The best way to discriminate between the different scenarios is a statistical study of different spatial and dynamical properties of jets.

One of the main goals underlying the launch of the X-Ray Telescope (XRT) aboard the Hinode satellite was to study magnetic reconnection in the corona by observing its different manifestations. With the advantage of the highest angular resolution ($1''.03$) compared to any solar X-ray mission and a broad range of detectable temperatures ($6.1 < \log_{10} T < 7.5$), XRT is ideally suited for studying both the statistical properties of jet parameters and modeling individual events (Golub et al. 2007; Kano et al. 2007). In this work we present the first study of polar jets, which clearly demonstrates the high frequency of events in the coronal holes. We concentrate on a statistical examination of different jet parameters: the apparent outward velocity, transverse velocity, width, maximum height, duration, spatial distribution, and inclination. A statistical analysis on transverse motions of the jets is also novel. Such motion was noticed before (Shibata et al. 1992), but no statistical work had been performed before.

In 2006 November, 2007 January, and 2007 March, XRT participated in an extensive study of reconnection events in both polar coronal holes. For the following analysis we use data taken during the 2007 January run of the SOHO/Hinode campaign 7197, which looked at the South pole coronal hole. In the next section we present our dataset, and then discuss the methods used to determine the different jet parameters as well as the results from the statistical analysis.

2. Observations

SOHO/Hinode campaign 7197 was run between 2007 January 08 and January 21. For 6–12 hours on each of these days, XRT took high-cadence observations of the South-pole coronal hole in two different filters — Aluminum (Al_poly) and Titanium polyamide (Ti_poly). The Al_poly filter was used for 4–7 hours every day, and the rest of the data were taken in Ti_poly. The maximum of the temperature response of the Al_poly filter is about 7 million degrees (with a significant peak at 1 million degrees as well), and that of the Ti_poly filter is close to 8 million K (Golub et al. 2007). In this work we present an analysis conducted only on images taken in the Al_poly filter in the interval January 12–19. All images during this time were 1024×512 pixels, or $1053'' \times 526''\!.6$, taken at 30 s cadence, and centered on the South pole. A movie of one observational day of data can be found at a web site.[1]

Jet events were selected according to the following 2 criteria: visible ejection of material on a timescale of several tens of minutes; a rapid increase in the length of the brightness enhancement (associated with a jet) with time. We selected a total of 104 events that by visual inspection of a log-scaled movie sequence satisfied the above conditions. This number of jets was accumulated within 44 hours of observation, which for the first time demonstrates the high frequency of these events. During this time the events were almost evenly distributed with time, although we often observed that jets occured in spatial and temporal clusters of 3–4 events. There were also some jets that reoccurred 2–3 times in the course of 1–4 hours.

We selected a subset of images around each jet event. Each subset included all separate stages of a jet event, starting with the emergence of a bright dipole, going through a reconnection event, and ending with a relaxation of the loop structure after the jet. Following the above prescription, we produced 104 subsets, covering time intervals of between 5 min and 2 hr. All images were cut to a size of 20 pixels by 30 to 200 pixels, depending on the event, in order to make the subsequent analysis easier. On all data subsets we applied initial image preparation and cleaning techniques. All images were processed for different kinds of instrumental noise and cosmic particle hits. All data were also normalized by exposure time. In figure 1, we give an example of a jet that was observed in the Al_poly filter at 13:11 UT on January 17. The image shows the moment when the jet had reached the maximum length (or height, as we call it later). The underlying double-loop structure is quite distinguishable.

3. Outward Velocity Determination

The first parameter that we discuss here is the apparent (plane of the sky) outward jet velocity. We put a lot of effort in analyzing this parameter, since it is most commonly used to distinguish between different mechanisms of ejection of material (Shimojo et al. 1996). All methods that we discuss next are used to measure the velocity of the intensity front.

3.1. *Image Processing*

After each image was initially processed, we applied a Laplacian edge-detection filter with $\sigma = 2$ pix on the cleaned and normalized image, and then added back the resultant image to the Gaussian-smoothed (same σ) original image. In this way, a considerably sharpened and denoised imaged was produced. In figure 2, you can see the same frame as that shown in figure 1, but after the post-processing just described. In this way we end up with two separate datasets — one that is just initially processed for noise and particle hits (dataset I), and one that has been smoothed and sharpened (dataset II).

3.2. *Methods*

Four different methods were developed for determining the apparent outward velocities of the jets. The first three methods give consistent results. The first method we discuss here is fairly straightforward, and we refer to it as the 'stack plot' method. The next two methods use the same basic idea, but with different variations. The fourth method relies on a different concept. Since the first three methods are based on spatially averaging the width of the box around the jet, they are incapable of detecting material moving at high speeds on the order of the Alfvén speed. Such small intensity enhancements will remain unresolved after width-averaging, and hence the higher velocity component will remain hidden. Thus, we find that the first three methods are suitable for studying bulk velocities that are smaller, or on the order of the speed of sound in the plasma. The fourth method that we discuss is sensitive to larger velocities, and hence sometimes give different results from the first three methods.

The first three methods give velocity estimates in the range of $70\,\mathrm{km\,s^{-1}}$ to $400\,\mathrm{km\,s^{-1}}$. This result is consistent with previous statistical studies of jets (Shimojo et al. 1996; Shibata et al. 1992; Canfield et al. 1996; Dobrzycka et al. 2002). The last method sometimes detected higher velocities of about 600–$1000\,\mathrm{km\,s^{-1}}$, but they were not included in the statistical analysis, since the error bars on such velocities were usually very large, and we plan to examine the separate events carefully in another paper. In figure 4 one can see the velocity histogram distribution for 101 jets, for which we securely determined the velocities, sometimes using more than one method. The distribution peaks at about $160\,\mathrm{km\,s^{-1}}$ and an extensive wing towards higher velocities is present.

We found that different methods work best on different jets. When two or more methods were successfully applied on one and the same jets, the one with the smallest error was chosen.

3.2.1. *The "stack plot" method*

We applied the following method on images from dataset I. The idea behind the method is the following: Consider an image consisting of n columns and m rows. If one averages over the n elements of a given row one would get the width-averaged brightness at any distance from the base, m. Thus, for a given time, we obtained a single column to represent the whole image. Plotting such a column for every instance of time, we effectively produced a plot of the brightness with height and time (figure 3). Then, we fit a straight line to the left side of the bright region on the figure to obtain the apparent outward velocity of the jet. If we assigned physical units of seconds and kilometers to the X- and Y-axis of this plot, we obtained the velocity in $\mathrm{km\,s^{-1}}$. In all the cases, we successfully fit a straight line to the slope, which implies that the temperature of the material comprising the intensity enhancement does not change significantly during the events. The reason is that the temperature-response curve of the Al_poly filter is considerably flat (Golub et al. 2007), so for the transmitted intensity to drop 10 times, the temperature

[1] ⟨http://hea-www.harvard.edu/Solarb/XRT/www2/savcheva/firstjet.html⟩.

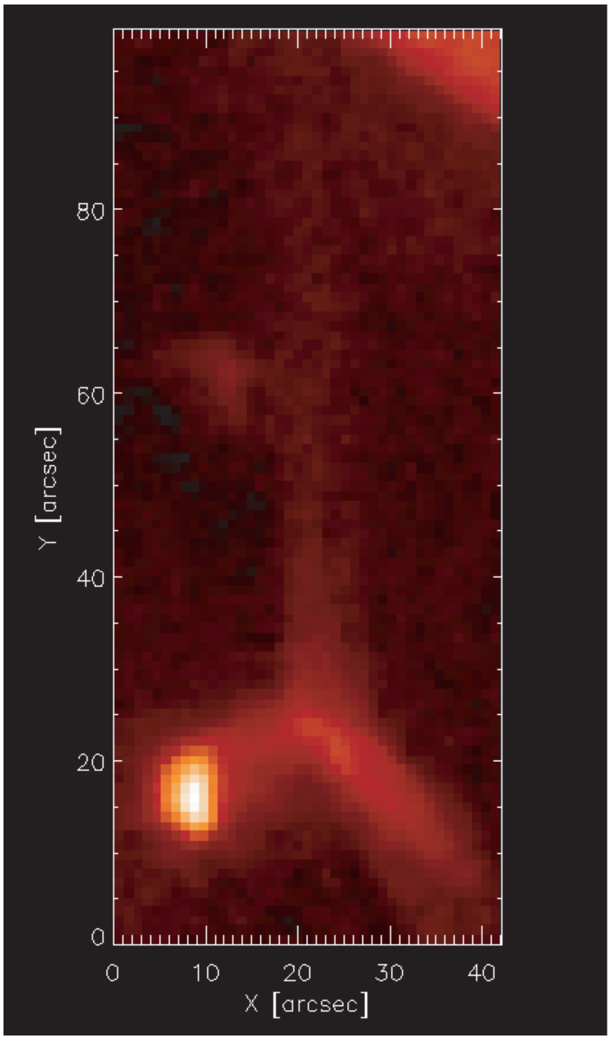

Fig. 1. Image of a polar coronal jet after the instrumental noise and cosmic particle hits had been removed. The image has also been normalized by exposure time and rotated vertically.

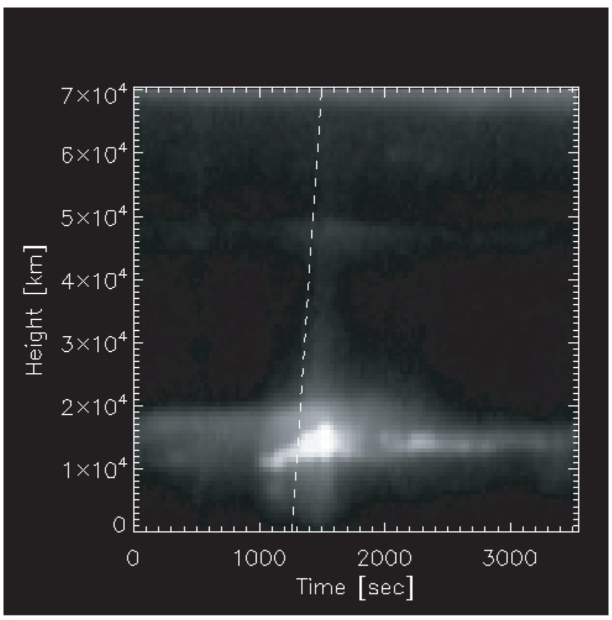

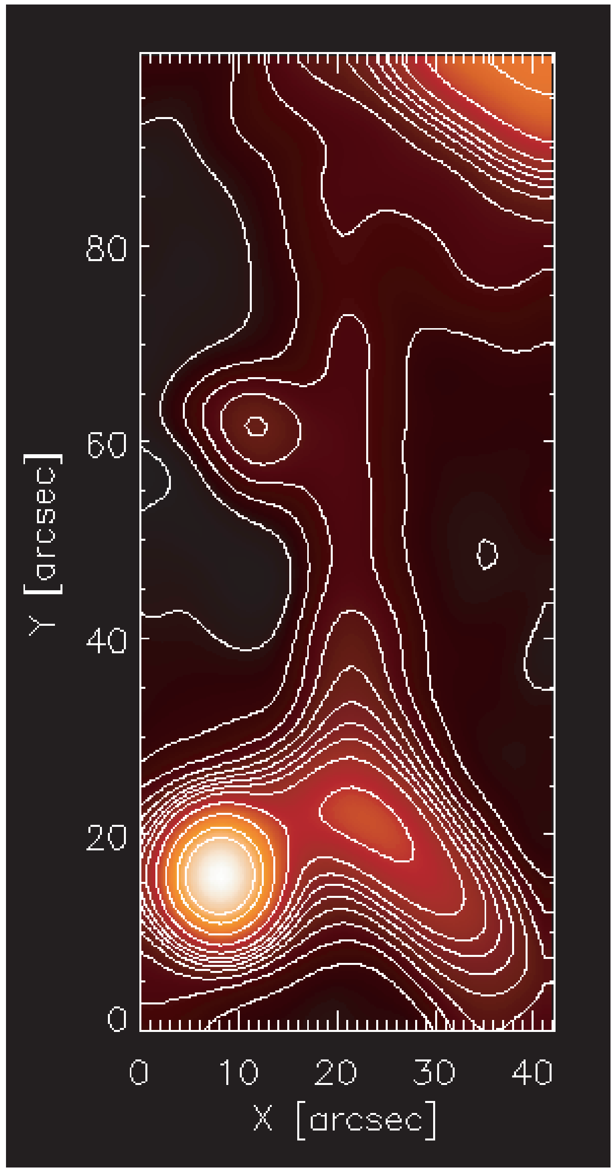

Fig. 2. Same image as shown in the previous figure after Gaussian low-pass and Laplacian edge-detection filters had been applied.

Fig. 3. Demonstrates the basic 'stack plot' method for velocity determination. A line has been fit to the left slope of the bright region.

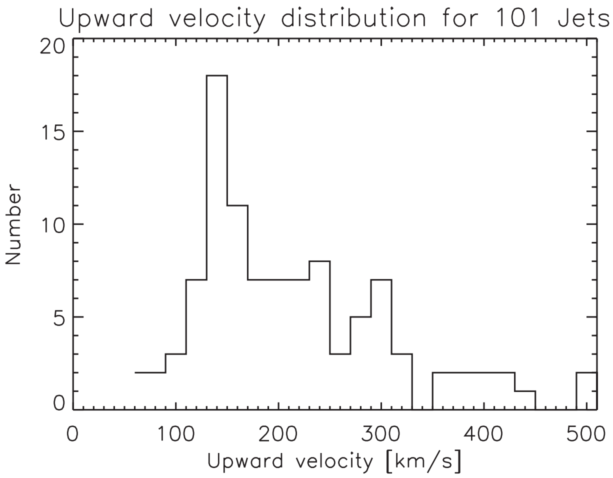

Fig. 4. Histogram distribution of upward jet velocities for 101 jets. Bin size is 20 km s^{-1}.

should change by 2×10^6 K. If we indeed have such a change in temperature, we would see a curvature to the slope, which would appear as a decelerating term. However, we did not observe such an effect, so we can infer that the temperature changes of the plasma were not very significant. One could explain the constant velocity by accelerating a constant-density plasma with decreasing temperature to make the line straight, but such a contrived situation we consider to be unlikely.

We successfully applied this method to 48 jets. This method proved to be useful for most of the brighter jets when the contrast between the jet and the background was relatively high. The error bar on the velocity given by this method (about 30 km s^{-1}) is somewhat higher than that given by the other methods.

3.2.2. "Difference stack plot" method

This method uses the same basic idea as the previous one in the sense that the result is a time-lapsed image where every column represents brightness of the jet with height at a given time. However, from each column, k, we now subtract the $(k+4)$-th, which corresponds to a future moment in time. Thus, we produce a time-difference plot.

Such a plot has the advantage that it takes away almost all background, even spatial gradients that otherwise would require some more complex techniques to remove. The method also highly amplifies the contrast between the jet and the background, and makes it easier to select the slope from which to extract the velocity. The largest number of jets was processed using this method — a total of 60. It also gives smaller error bars (about 10–15 km s^{-1}), and it is probably more precise as well. This method also works for most jets, although, when there is another bright feature overlaying the jet, one should be more careful.

3.2.3. Laplacian contour method

The method discussed here is a subsequent build-up on the "stack plot" method. It involves applying post-processing techniques onto the "stack plot" image, obtained as described in subsubsection 3.2.1. A Gaussian low-pass filter and a Laplacian operator are applied to the image. The image is scaled so that positive derivatives appear in white and negative in black. The contours corresponding to the $+/-$ or $-/+$ transition on the image are drawn, and a part of a contour is selected, which represents the left slope of the jet. Some judgment is required to choose part of the contour, which is not too erratic and does not cross itself. After selecting the first and last point of the desired part of the slope, we fit a line to the enclosed portion of the contour, and obtained an estimate of the velocity.

This method works best for jets where the outward flow appears to be uninterrupted by other brighter structures, and when the background is fairly smooth. This method proved to be useful for 36 events. Used with jets under the right conditions, this method gives smallest errors — about 5–10 km s^{-1}, and also involves the least judgment by the scientist. The method works well in most cases, except when the background is too erratic at small scales.

3.2.4. Brightness contour method

The brightness contour method is entirely different. Here, we consider every image from dataset II. We then draw isocontours of different brightness levels. To determine the velocity we plot the vertical position of the highest point of a given contour (measured from the base of the image) with time and fit a line to it. The maximum of the contour may not behave very well spatially and temporally, so we choose another four points, equally spaced along the contour, and repeat the analysis, thus increasing the statistical significance of the method.

It is important to note that in some cases this method gave consistent results with the other three methods, although usually with larger error bars. In the remaining cases, the velocities that it yielded were systematically higher — around 600–1000 km s^{-1}. This method produced consistent results for 27 jets. As mentioned above, we think that the fact that this method involves no averaging along the width of the box, it actually gives us an estimate of another type of velocity on the order of the Alfvén speed. This may give us an insight into a different process, e.g., pressure-driven evaporation flow (Shimojo et al. 1996), which we plan to examine in another study.

We chose to discuss this method last because all other parameters that we study are derived from the same type of brightness contour analysis.

4. Other Jet Parameters

4.1. Heights

When deriving the remaining parameters, we will always use dataset II and base our analysis on the brightness contour method described above. In order to find the height of the jet, we need to develop a method for finding the front of the jet. Each jet can be confined inside a given brightness contour. We first select a reference jet. From all images of both subsets of the reference jet and the jet at hand, we subtract the first image of the corresponding subset, where there is still no jet present. In this way we effectively reduce the bias from the background. We choose the contour on the reference jet to have a value $10^{4.5}$. The corresponding contour on the other jet is then given by $C = C_{\mathrm{ref}} J / J_{\mathrm{ref}}$. Here, J is the average brightness of each jet, when the jet has reached the maximum

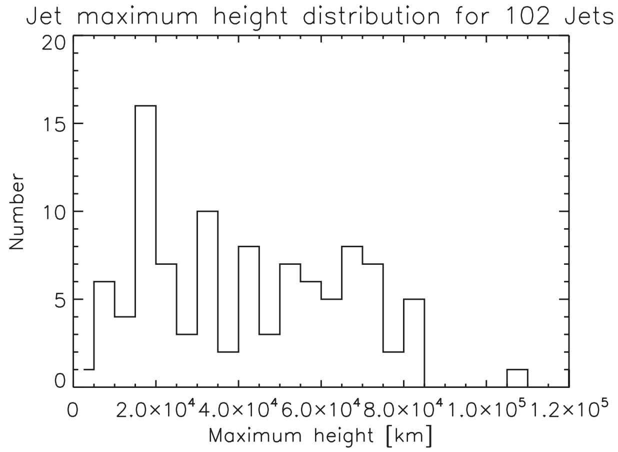

Fig. 5. Histogram distribution of the jet maximum heights for 102 jets. The bin size is 5000 km.

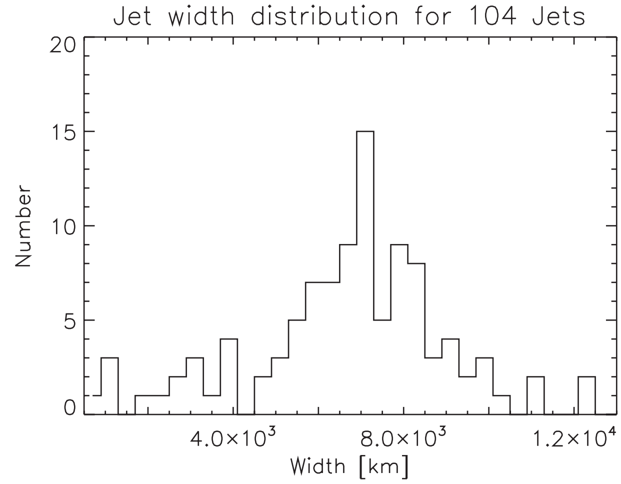

Fig. 6. Histogram distribution of jet widths for 104 jets. Bin size is 500 km.

height. $J_{\rm ref}$ is the averaged brightness of the reference jet. As defined, the height of the jet is determined by the transmissivity of the Al_poly filter to emission from the plasma with a certain density and temperature. The jet does not terminate at the height that we measure, but rather its brightness falls sharply at that height because its density and/or temperature decrease as it extends further into the heliosphere. After we have done this, we simply follow the vertical position of a given brightness contour with time and record its maximum values.

The heights derived in this way are all in the range of (1.0—12) $\times$ 10^4 km, which is consistent with previous statistical works on jets (Shimojo et al. 1996). While the study of Shimojo et al. concentrated mainly on larger jets, partly as a selection effect from the limited resolution of Yohkoh, we have a much better sample with smaller lengths, with a local peak at 1.8×10^4 km. In figure 5 we show the distribution of heights for 102 jets, for which the code converged.

4.2. *Collimated Widths*

Along with the jet heights, we calculated the widths of the jets at several points along their length. In this study we considered only the height-average width of the jet above a certain height. We decided to do that, since many authors have noticed that jets appear to be highly collimated above a certain height above the base (Shimojo et al. 1996; Shibata et al. 1992). We determined these collimated widths. We found several events of converging and twisting jets. Then, defining and measuring the width is a more complicated matter, so we decided to set their width to be the width at 2/3 the distance from the base.

Here, we also worked with dataset II with the first image of a subset subtracted from all other images in order to reduce the background. To determine the width of a jet at some height, we took a horizontal cross section of the jet. The logarithm of the brightness profile, $b(m)$, of that cross section we interpret as a probability distribution, $p(m)$, that needs to be normalized. Thus, $p(m) = b(m)/\sum_m b(m)$, and therefore the width of the jet is given by $w = \sqrt{\sum_m [p(m)m^2] - [\sum_m p(m)m]^2}$. Since this calculation is done on a Gaussian-smoothed image, we then applied a small correction to the result, subtracting the variance of the Gaussian used for smoothing.

The result of this calculation was that the jet widths lie well in the range between 6×10^3 km and 10^4 km with just a few exceptions. This result is slightly different from the sizes Shimojo et al. reported again, because they selected mainly larger jets. In figure 6 one can see the histogram distribution of the jet-collimated widths for all 104 jets.

4.3. *Transverse Velocities*

While working on the other characteristics, we noticed that most jets exhibited a substantial transverse motion, in the plane of the sky, sideways, along the underlying loop structure. Here, we attempted the first statistical analysis of this motion, it was merely mentioned by other authors (Shibata et al. 1992). We calculated these velocities in the same way that we calculated the outward velocities, by using only the brightness contour method. By looking at the motion of the maximum of a given contour in the transverse direction with time and fitting a line to it, we determined the value of the velocity of the transverse motion when it is constant. We often observed some acceleration and deceleration before and after a period with constant transverse motion.

The transverse velocities vary between 0–35 km s^{-1}, which is highly consistent with previous statements about this kind of motion (Shibata et al. reports 10–20 km s^{-1}). In figure 7 we show the distribution of transverse velocities. Note that the peak at 0 km s^{-1} is artificially high, since some jets have error bars that are too big around 0 km s^{-1}. We observed that most of the closed field structures in the coronal hole were oriented in the East–West direction, and that the jet apparent transverse velocities were also in the East or West direction. In the figure, negative velocities are pointing to the West and positive are to the East.

4.4. *Lifetimes*

The lifetimes of the jets were also a characteristic that was easily determined, at no cost, in the process of estimating other parameters. We defined the beginning of the jet to be the moment when a little spike of brightness starts to emerge

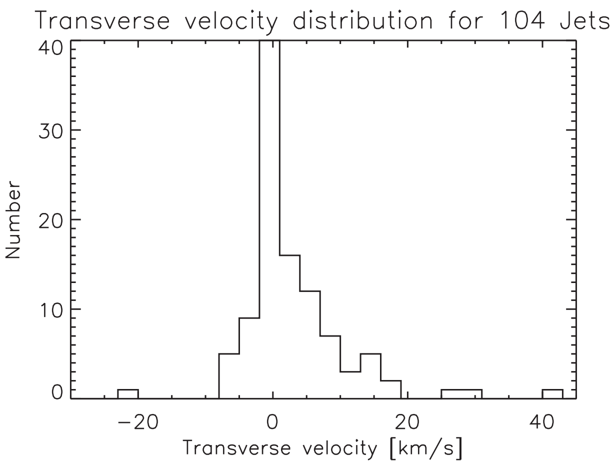

Fig. 7. Histogram distribution of the jet transverse velocities for 104 jets. The bin size is $2\,\mathrm{km\,s^{-1}}$. The peak at $0\,\mathrm{km\,s^{-1}}$ is artificially high, since the transverse velocities around $0\,\mathrm{km\,s^{-1}}$ of many jets have large uncertainties.

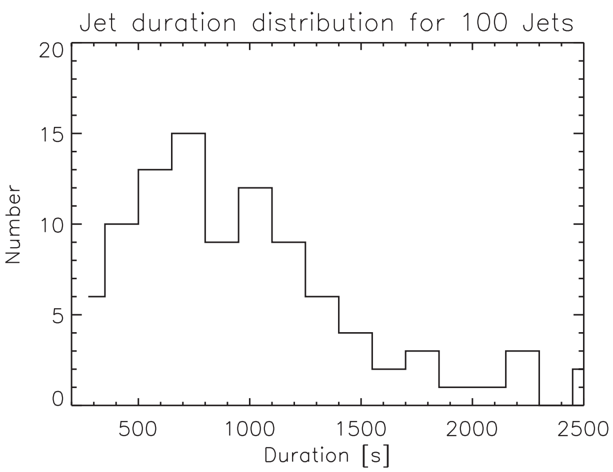

Fig. 8. Histogram distribution of jet durations for 100 jets. The bin size is 150 s.

from the reconnection site, and becomes visible, which visually coincided with a huge and very rapid increase of the brightness of the smaller bi-pole. Similarly, the end of the jet was set to be the moment when the contrast between the jet and the background disappears. In this sense, the lifetime of the jets that we determined encompassed the reconnection event and propagation of the jet. All of these times were determined by eye using an animated sequence of images. Being consistent with our initial criterion for a jet event, most jets proved to last for several minutes to several tens of minutes. Again, to compare with Shimojo et al., our sample was slightly different, since their worse temporal resolution did not allow the detection of many short events that we have in our dataset. It can be seen from the histogram plot that the jet lifetimes peak at about 10 min (figure 8). We did not observe any obvious correlation between the jet size and the lifetime.

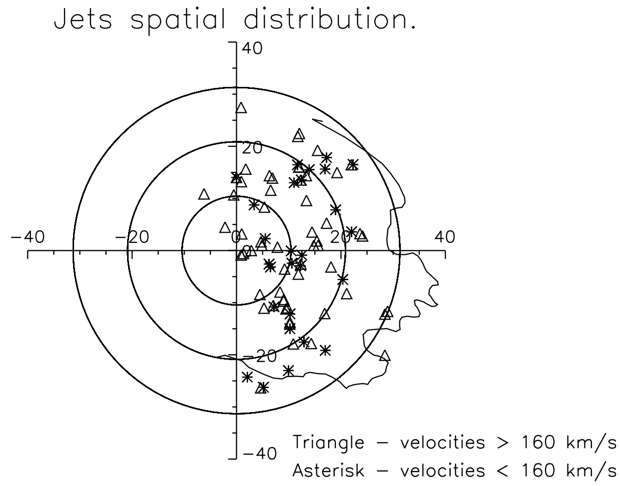

Fig. 9. Jet positions on the solar disk as viewed from the South pole. The circles correspond to fixed latitudes of 0° is the South pole. The jet velocities are symbol-coded to show the distribution of upward velocities with position—triangles are velocities $>160\,\mathrm{km\,s^{-1}}$ and asterisks are velocities of $<160\,\mathrm{km\,s^{-1}}$. The boundary of the polar coronal hole is also shown.

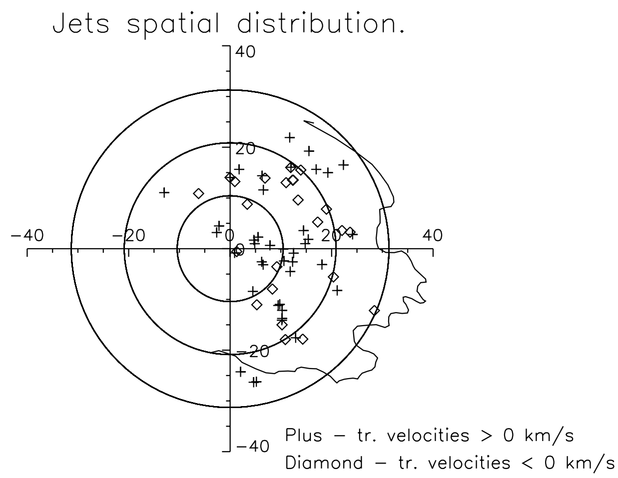

Fig. 10. Jet positions on the solar disk as viewed from the South pole. The circles correspond to a fixed latitudes of 0° is the South pole. The jet transverse velocities are symbol-coded to show the distribution of these velocities with the position; the plus symbol is the transverse velocity $>0\,\mathrm{km\,s^{-1}}$; the diamond is a velocity of $<0\,\mathrm{km\,s^{-1}}$. The boundary of the polar coronal hole is also shown.

5. Jets and the Polar Coronal Hole

While making data subsets for every jet we obtained information about the position of the jets in pixel coordinates and their inclinations. Fitting the limb of the sun to all jet images allowed us to extract the heliocentric coordinates of the origin of the jet stream. We then chose the last image from the January 19 and rotated all jet positions to this time — 17:02 UT. We plotted the rotated position onto a representation of the solar disk, as viewed from the South pole (figure 9).

As expected, all jets were confined near to the South pole in the hemisphere facing the Earth, since the dataset was one week long.

We also extracted the boundary of the South pole coronal hole, as seen in the Al_poly filter on the January 17 (the middle of our dataset), and rotated it to the same time as the jets were rotated to. After we plotted the boundary of the coronal hole on the same plot (figure 9) we saw that almost all jets fell strictly inside it, which is consistent with what we observed while selecting the events from the animated image sequence. It is important to note that the boundary of the coronal hole changed shape and size during the time of the observation. Since we plotted only the boundary of the coronal hole at one moment, it is easy to see how some jets may appear slightly outside it in figures 9 and 10. It is established that jets that form outside the coronal holes, in a closed surrounding field, are smaller, have a more curved shape, and are rarer. Since the configuration of the field lines change dramatically from open to closed across the boundary of the coronal hole, and hence the setting for reconnection also changes, we exclude the possibility of a smooth distribution of events across the boundary. The distributions in figures 9 and 10 clearly demonstrate this.

We plotted the jet apparent outward and transverse velocities, symbol-coded with the positions. In figure 9, slower jets with velocities of $< 160\,\mathrm{km\,s^{-1}}$ are plotted with asterisks, and faster jets, with velocities $> 160\,\mathrm{km\,s^{-1}}$ are plotted with triangles.

In figure 10 jets with positive velocities are plotted with pluses, and jets with negative velocities with diamonds. Both spatial distributions show no obvious dependence of the value of the velocity on the jet position relative to the coronal hole boundary.

6. Conclusion and Discussion

This preliminary work describes the fundamental physical properties of jets seen in both polar coronal holes. We describe methods for accurately measuring the jets' velocity, length, durations, and width. The motivation behind this work is to study those events that may turn out to constitute an important and substantial component of the high-speed solar wind, and also to represent a clear and unambiguous example of magnetic reconnection. As such, they are worthy of a detailed and ongoing investigation. Morphologically, similar jets have now been seen in high resolution Hinode Ca II observations, which may give us further insight into the basic physics underlying these beautiful events.

This particular analysis was conducted on data collected during the Hinode/SoHO campaign 7197, between 2007 January 12 and 19. This study showed that X-ray jets are fairly common in the solar corona, rather than being exotic and rare events.

For determining the apparent outward velocity, we developed four methods. We discussed that when using spatial averaging, the detectable velocities are smaller, or on the order of c_{s}. We obtained that the histogram distribution for the apparent outward velocity of the jets peak at about $160\,\mathrm{km\,s^{-1}}$. These results can be used to point to the mechanism for expansion of the jet, namely a pressure-driven expansion of the plasma. The different possible models that can explain these results are not in the scope of the current work; here, we merely report on the results from our statistical analysis. More observations of reconnection events with different types of instruments and at different heights in the heliosphere are necessary for a progress on the reconnection jet problem. This requires a continued committed study using all of the Hinode instruments.

We carried out the first statistical consideration of the jet transverse velocity. We defined this to be the velocity of the translational motion of the jet in a direction perpendicular to its elongation. We obtained velocities in the range of 0–$35\,\mathrm{km\,s^{-1}}$, which is consistent with Shibata et al. (1992). According to their work, such motion can be well explained by a reconnection site sliding sideways atop the magnetic bi-poles. From the fact that these transverse motions are so common, we can obtain more insight, and even constrain different reconnection scenarios.

We also derived that the height, width, and lifetime have mean values of about 50000 km, 8000 km, and about 10 min, respectively. All of the above results are consistent with previous studies of jets (Shimojo et al. 1996; Shibata et al. 1992; Canfield et al. 1996; Alexander & Fletcher 1999). However, the much finer spatial and temporal resolutions of XRT, as compared to SXT/Yohkoh, lead to a larger sample of jets of many different sizes and lifetimes.

We also demonstrated that most jets are situated inside the polar coronal hole. We did not notice any correlation between the jet parameters and their positions relative to the coronal hole boundary. The association of jets with the boundary of the coronal hole is intriguing due to a possible relationship of the jets with the evolution of the boundary. This will be better studied when equator-to-pole coronal holes appear on the Sun.

The relationship of jets to X-ray Bright Points (XBPs) also needs to be established. Many XBPs are formed from the convergence of unrelated magnetic elements in the quiet Sun (Webb et al. 1993; Priest et al. 1994). The basic jet model is dependent on the emergence of a bi-pole into a unipolar region. Detailed magnetometery is needed to understand the relationship of the magnetic flux evolution to jets and bright points in coronal holes.

The connection between X-ray jets and Hα surges has also been broadly studied (Yokoyama & Shibata, 1995; Canfield et al. 1996). However, a statistical study of this relationship has not yet been conducted. More studies of X-ray jets must be coordinated with studies of the same events at other wavelengths, and hence other heights in the solar atmosphere, in order to further explore the underlying magnetic morphology and physical processes.

During this study, some interesting events were selected. Those events along with a more thorough analysis of the parameters discussed above as well as other characteristics will be studied in future work to constrain the model for the reconnection and ejection and expansion of material.

Hinode is a Japanese mission developed and launched by ISAS/JAXA, collaborating with NAOJ as a domestic partner, NASA and STFC (UK) as international partners. Scientific operation of the Hinode mission is conducted by the Hinode science team organized at ISAS/JAXA. This team mainly consists of scientists from institutes in the partner countries. Support for the post-launch operation is provided by JAXA and NAOJ (Japan), STFC (U.K.), NASA, ESA, and NSC (Norway).

References

Alexander, D., & Fletcher, L. 1999, Sol. Phys., 190, 167
Canfield, R., Reardon, K., Leka, K., Shibata, K., Yokoyama, T., & Shimojo, M. 1996, ApJ, 464, 1016
Dobrzycka, D., Cranmer, S. R., Raymond, J. C., Biesecker, D. A., & Gurman, J. B. 2002, ApJ, 565, 621
Golub, L., et al. 2007, Sol. Phys., 243, 63
Kano, R., et al. 2007, Sol. Phys. in press
Priest, E., Parnell, C., & Martin, S. 1994, ApJ, 427, 459
Shibata, K., et al. 1992, PASJ, 44, L173
Shimojo, M., Hashimoto, S., Shibata, K., Hirayama, T., Hudson, H., & Acton, L. 1996, PASJ, 48, 123
Strong, K. T., Harvey, K., Hirayama, T., Nitta, N., Shimizu, T., Tsuneta, S. 1992, PASJ, 44, 161
Webb, D., Martin, S., Moses, D., & Harvey, J. 1993, Sol. Phys., 144, 15
Yokoyama, T., & Shibata, K. 1995, Nature, 375, 42